

High-speed and Low-energy Actuation for Pneumatic Soft Robots With Internal Exhaust Air Recirculation

Miao Feng^{1,2}, Dezhi Yang^{1,2}, Carmel Majidi³, and Guoying Gu^{1,2,4}

¹Robotics Institute, School of Mechanical Engineering, Shanghai Jiao Tong University, Shanghai, 200240, China.

²State Key Laboratory of Mechanical System and Vibration, Shanghai Jiao Tong University, Shanghai, 200240, China.

³Soft Machines Lab, Carnegie Mellon University, Pittsburgh, PA 15213, USA.

⁴Meta Robotics Institute, Shanghai Jiao Tong University, Shanghai, 200240, China.

September 27, 2022

Abstract

Multi-chamber soft pneumatic actuators (m-SPAs) have been widely used in soft robotic systems to achieve versatile grasping and locomotion. However, existing m-SPAs have slow actuation speed and are either limited by a finite air supply or require energy-consuming hardware to continuously supply compressed air. Here, we address these shortcomings by introducing an internal exhaust air recirculation (IEAR) mechanism for high-speed and low-energy actuation of m-SPAs. This mechanism recirculates the exhaust compressed air and recovers the energy by harnessing the rhythmic actuation of multiple chambers. We develop a theoretical model to guide the analysis of the IEAR mechanism, which agrees well with the experimental results. Comparative experimental results of several sets of m-SPAs show that our IEAR mechanism significantly improves the actuation speed by more than 82.4% and reduces the energy consumption per cycle by more than 47.7% under typical conditions. We further demonstrate the promising applications of the IEAR mechanism in various pneumatic soft machines and robots such as a robotic fin, fabric-based finger, and quadruped robot.

Corresponding author(s) Email: guguaying@sjtu.edu.cn



Figure 1:

ToC Figure. [The internal exhaust air recirculation (IEAR) mechanism to simultaneously increase the actuation speed and reduce the energy consumption of pneumatic soft robots.]

1. Introduction

Multi-chamber soft pneumatic actuators (m-SPAs) are promising in the applications of soft machines and robots, including rotators (Ainla et al., 2017), oscillators (Preston et al., 2019), grippers (Shintake et al., 2018;

Gong et al., 2021; Low et al., 2020), robotic hands (Gu et al., 2021; Deimel and Brock, 2016), gloves (Feng et al., 2021; Connolly et al., 2019; Yun et al., 2017), snake-inspired robots (Qi et al., 2020; Luo et al., 2014), bioinspired robotic fish (Marchese et al., 2014), multi-legged robots (Drotman et al., 2021, 2017; Wehner et al., 2016; Tolley et al., 2014; Shepherd et al., 2011), and soft functional arrays (Hashem et al., 2021a,b; Robertson et al., 2017). Increasing the speed and reducing the energy consumption of m-SPAs could lead to more steady, reliable, and robust performance (Ainla et al., 2017; Marchese et al., 2014; Tolley et al., 2014; Aubin et al., 2022; Gorissen et al., 2017; Polygerinos et al., 2017; Xavier et al., 2022). However, most existing architectures are designed with limited consideration of actuation speed and energy consumption and instead generally focus on other performance metrics related to versatile degree-of-freedom (Wang et al., 2021), larger working space (Chen et al., 2021; Ke et al., 2021), higher force (Yap et al., 2016; Li et al., 2020), or smarter perception (Takaki et al., 2019; Zoller et al., 2018; Giffney et al., 2016).

To address these challenges, recent efforts have been dedicated to exploring variants of air pumps. These architectures can provide enhanced supplied air pressure and airflow by (i) connecting air pumps in series or parallel (Wehner et al., 2014), (ii) introducing a double-piston (Kim et al., 2018) or a double-acting pneumatic cylinder (Sridar et al., 2020) to compress more air in a compression cycle, or (iii) using a phase-change medium (dry ice, liquid CO₂, DME, etc.) as a pneumatic source (Okui et al., 2018; Wu et al., 2007). These pump variants indeed improve the actuation speed of m-SPAs, but they also introduce additional challenges related to complicated mechanical design and greater energy consumption.

Meanwhile, some low-power pumps have been developed as a promising alternative to reduce the energy consumption of m-SPAs. For example, based on charge-injection electrohydrodynamics (Cacucciolo et al., 2019) or dielectric fluid-amplified electrostatic zipping structure (Diteesawat et al., 2021), stretchable electro-pneumatic pumps are reported to operate with a low pump power of fewer than 1 W. However, they suffer from supplying low pressures of less than 10 kPa (Cacucciolo et al., 2019; Diteesawat et al., 2021) or small airflow (161 mL/min) (Diteesawat et al., 2021). Alternatively, some chemical pumps that utilize fuel combustion or decomposition (CH₄, H₂O₂, etc.) have been designed to provide high pressure ([?] 50 kPa). However, the refueling process and low airflows ([?] 50 mL/min) make them unfeasible to build a compacted low-power system for practical applications (Tolley et al., 2014; Stergiopoulos et al., 2014). Therefore, achieving high-speed and low-energy actuation of m-SPAs remains an open challenge (Table S1 and Figure S1a) (Marchese et al., 2014; Drotman et al., 2021; Shepherd et al., 2011; Aubin et al., 2022; Wehner et al., 2014; Mosadegh et al., 2014; Joshi and Paik, 2021; Lee et al., 2021; Gong et al., 2016; Yang et al., 2018; de Pascali et al., 2022).

Figure 1. Working Principle of Internal Exhaust Air Recirculation (IEAR). **a** The working principle of IEAR. Inlet to inflate the chamber Outlet to deflate the chamber Branch for internal recirculation Branch to the atmosphere Closed branch for external recirculation. We have DIDO(), IEAR(), and EEAR(). IEAR recirculates compressed air by a valve island. Compared with DIDO, IEAR recycles compressed air and recovers internal energy. Compared with EEAR, IEAR does not require an air buffer and air recompression by the pump. **b** The pressure-volume relationship (constant temperature, open system). With IEAR, exhaust air is directly transmitted and recirculated between chambers through a specialized valve island, thereby shortening the working cycle (the arrow path) and reducing energy loss. **c** Traditionally, compressed air directly inlet and directly outlet (DIDO) the chambers of m-SPAs, leading to markedly energy loss and poor actuation performance (speed, energy efficiency, supplied pressure, system power, etc.).

Rich media available at <https://youtu.be/-HbTS0rmIis>

Movie S1. The traditional DIDO mechanism

In tackling this challenge, it is important to note that most state-of-the-art m-SPAs utilize a “direct ac-

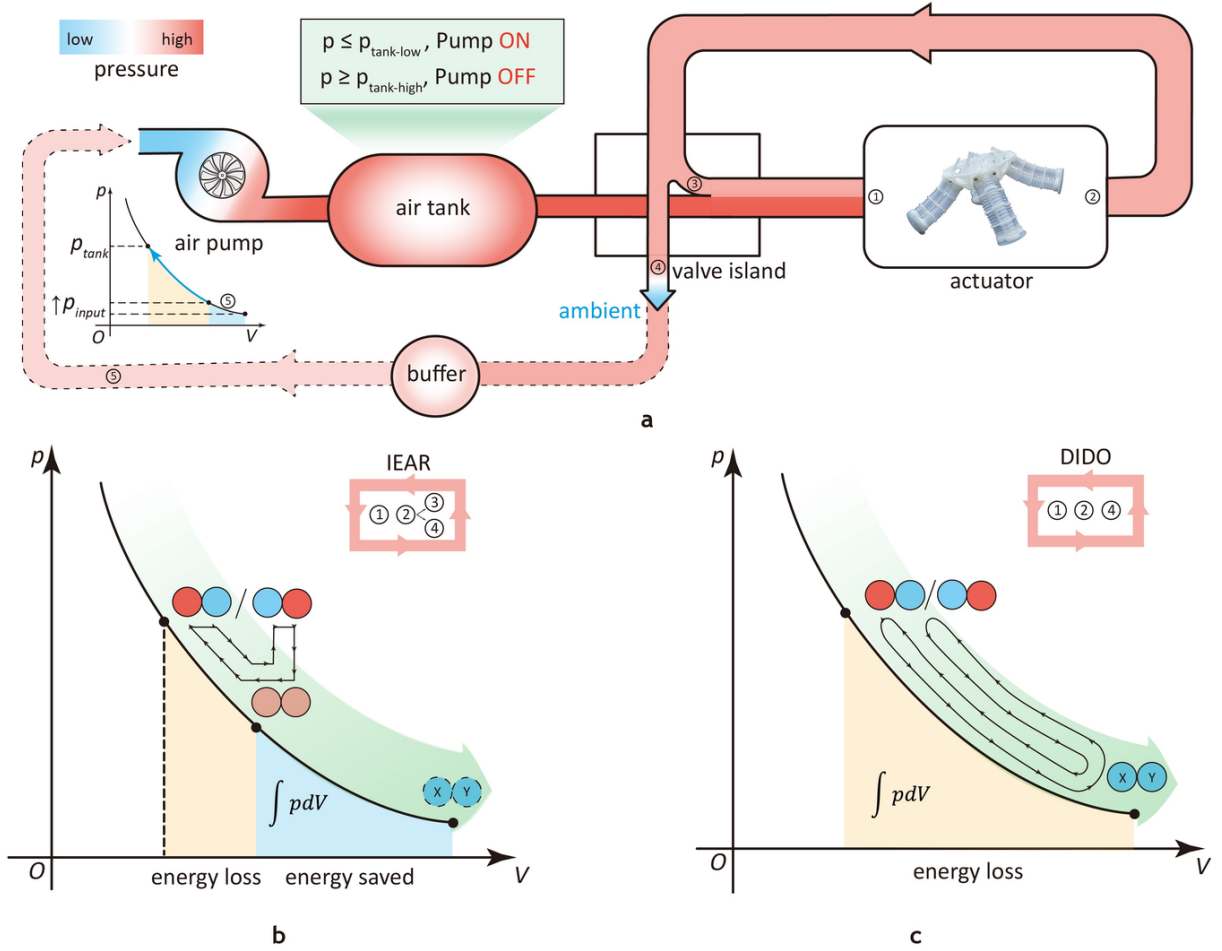


Figure 2:

tuation” mechanism in which compressed air enters the actuator directly through an inlet and leaves directly through an outlet to an ambient environment (termed DIDO, **Figure 1a**, **Figure S1b**; and **Movie S1**) (Joshi and Paik, 2021; Xavier et al., 2021; Zhang et al., 2021). As a result, the internal energy stored in the exhaust air for the DIDO mechanism cannot be recovered. For higher energy efficiency, an optional method is to reduce the input work of the system by improving the inlet pressure of a pump (Chou and Hannaford, 1996). For example, an air pump can recompress the exhaust air with residual pressure to a target pressure through an external exhaust air recirculation (EEAR, **Figure 1a**) mechanism (Wehner et al., 2014; Lee et al., 2021), where an extra pneumatic buffer (e.g., Re-Air valve) can be used to reduce severe pressure fluctuation (Lee et al., 2021). However, a key limitation is that this mechanism depends on the incorporation of pumps that typically have low electrical-to-mechanical energy conversion efficiency and, therefore, consume excess energy when recompressing the exhaust air. In addition, this mechanism lacks consideration of the actuation speed of m-SPAs (**Figure S1b**). Based on the architecture of EEAR, some researchers also achieve impressive programmable output pressure by replacing the pneumatic buffer with a group of air regulators, while actuation speed or efficiency is not considered in applications (Zhang et al., 2021).

In this work, we introduce an internal exhaust air recirculation (termed IEAR, **Figure 1a**) mechanism for high-speed and low-energy actuation of m-SPAs that overcomes these existing challenges. Through

the rhythmic actuation of multiple chambers following a shortened energy path, our IEAR mechanism can recirculate the exhaust compressed air from one chamber to another through a specialized valve island. In contrast to other existing methods based on air recirculation, this approach avoids the need for pump-controlled air recompression. Moreover, we introduce a dynamic model of m-SPAs to guide the analysis of our IEAR mechanism, with theoretical predictions that reasonably agree with the experimental measurements. Building on previous studies that examined the dynamics of pneumatic actuators with a single chamber (Joshi and Paik, 2021; Lee et al., 2021; Joshi et al., 2021; Xavier et al., 2020), our dynamic model is valid for actuators with multiple pneumatic chambers.

Characterization focuses on two exemplary embodiments of m-SPAs: an actuator with two chambers (Double Bellows) and an actuator with three chambers (Triple Bellows). These studies show that with IEAR, the actuation frequency for these two classes of m-SPAs can be improved by 82.4%-91.2%, while the energy consumption per cycle is reduced by 47.7%-51.2% under typical conditions. We further demonstrate the broad applications of the IEAR mechanism in various soft robotic systems, such as a robotic fin, fabric-based finger, and quadruped robot, for improving the actuation speed and reducing energy consumption. This work demonstrates that our IEAR mechanism plays a promising technology in the high-speed and low-energy actuation of m-SPAs for soft machines and robots.

2. Results

2.1 Working principle of the IEAR mechanism

The principle of our IEAR mechanism is illustrated in **Figure 1**. Unlike the traditional DIDO mechanism, the IEAR mechanism (**Figure 1a**) can recirculate the exhaust compressed air between the chambers. Taking a pair of chambers X and Y as an example, we can describe the actuation rhythms of our IEAR mechanism with the following steps (**Figure 1b**): (i) We begin by using compressed air stored in the air tank to inflate X to a set working pressure p_{high} ; (ii) Next, we open the valve between X and Y to transmit the compressed air from X to Y; (iii) When the pressure difference between X and Y is lower than a threshold Δp , we then close the valve; (iv) The chamber X continues deflating to p_{low} , while the air tank takes over the inflating process to pressurize Y to the set working pressure p_{high} . By exchanging the roles of X and Y, we repeat the steps i-iv to complete a working cycle. Since working cycles in practical applications can generally be approximated as an isothermal process (open system), the integral $\int pdV$ can be used to determine the change in internal energy of the compressed air. In this sense, our IEAR mechanism essentially shortens the working cycle (i.e., the energy path), avoids the high energy loss observed in the traditional DIDO mechanism (**Figure 1c**), and leads to enhanced air supply, thus improving the actuation speed.

In our IEAR mechanism, the working state of the air pump is independent of these specific actuation processes (**Figure 1a**). When the pressure in the air tank p_{tank} is less than a threshold $p_{tank-low}$, the air pump starts to work. Once p_{tank} is more than $p_{tank-high}$, the air pump turns off. The difference between $p_{tank-high}$ and $p_{tank-low}$ is the pressure tolerance for pump resting. Notably, we generally set the gauge pressure $p_{tank-low}$ and $p_{tank-high}$ as 120 kPa and 125 kPa, respectively.

To implement the IEAR mechanism, we develop an experimental platform (**Figure S2a**) that mainly consists of an air pump and an air tank (1 L) to provide compressed air, a valve island fabricated by a set of solenoid valves to control the rhythmic actuation of m-SPAs, and a dSPACE controller (sampling frequency, 1 kHz) to operate the ON/OFF states of the solenoid valves. The detailed air passage network of a three-channel valve island is presented in **Figure S2b**.

2.2 The dynamic model of m-SPAs

To guide the actuation performance analysis of the IEAR mechanism, we develop a dynamic model of m-SPAs based on the Clapeyron Equation. (See **Supplementary Note 1** and **Figure S3**).

For m-SPAs with n chambers, we can express the dynamic model as

$$\dot{\mathbf{p}} = \xi \left[\text{diag}(\mathbf{V}) + \text{diag}(\mathbf{p}) \frac{\partial \mathbf{V}}{\partial \mathbf{p}} \right]^{-1} \mathbf{Q} \quad (1)$$

$$\xi = \frac{\rho RT}{M}$$

(2)

where $\mathbf{p} = [p_1 \text{ amp}; p_2 \text{ amp}; \dots \text{ amp}; p_n]^{[?]}$, $\mathbf{V} = [V_1 \text{ amp}; V_2 \text{ amp}; \dots \text{ amp}; V_n]^{[?]}$, and $\mathbf{Q} = [Q_1 \text{ amp}; Q_2 \text{ amp}; \dots \text{ amp}; Q_n]^{[?]}$ represent the vectors of the pressure inside the chamber, chamber volume, and mass flow into each chamber, respectively. The parameters ρ, R, T, M are the air density under the standard conditions (1.293 g·L⁻¹, 0, 101.325 kPa), the ideal gas constant (8.314 J*mol⁻¹*K⁻¹), the absolute temperature, and the molar mass of air (28.9634 g*mol⁻¹), respectively.

Due to the lightweight of most soft actuators (Joshi and Paik, 2021; Lee et al., 2021; Xavier et al., 2020), we ignore the actuator mass and hypothesize that the volume is a function of air pressures. In this manner, we can express V_i as a function of the internal pressures

$$V_i = f_i(\mathbf{p}) \quad (3)$$

Thus, we can use the Jacobian matrix of chamber volume $\frac{\partial \mathbf{V}}{\partial \mathbf{p}}$ to determine the effects of air pressure change on volume change and the interaction between the chambers.

The dynamic model of m-SPAs implies that a shortened energy path resulting in a reduced range of pressure to follow and an improved mass flow for a reinforced \dot{p} can increase the actuation speed of m-SPAs, unveiling our IEAR mechanism's theoretical essence.

2.3 IEAR in m-SPAs with two chambers

To validate the use of the IEAR mechanism for pneumatic actuation, we first use the following exemplary architecture: m-SPAs with two chambers, which we term the Double Bellows (25.4 g, 150 mm). This validation study is used to verify the dynamic model and the ability of our IEAR mechanism to achieve high-speed and low-energy actuation (**Figure 2**; **Movie S2** and **3**).

Figure 2. m-SPAs with two chambers-Double Bellows. **a** Structure of the Double Bellows. **b** Arc-shape deformation geometry of the Double Bellows. **c** Equivalent section force diagrams of the Double Bellows. **d** Working flow chart of DIDO. When the conditions along the arrows are satisfied, the actuator moves to the next stage. **e** Working flow chart of IEAR. **f** Experimental pressures and theoretical pressures of DIDO and IEAR in 0-3 s. $p_{low} = 10$ kPa, $\Delta p = 10$ kPa. **g** Steady-state actuation frequency with p_{high} from 50 to 100 kPa. **h** Steady-state energy consumption per cycle with p_{high} from 50 to 100 kPa.

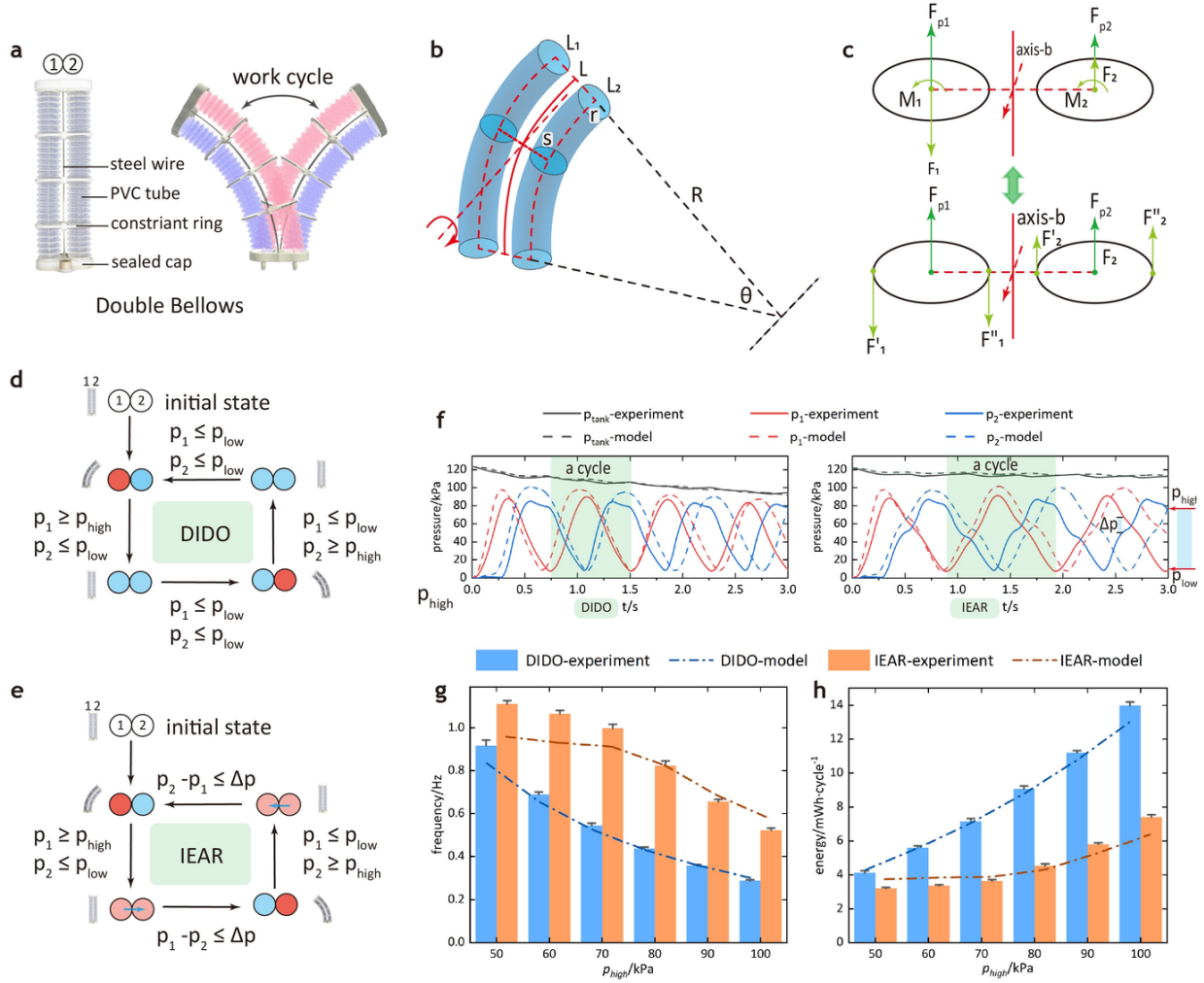


Figure 3:

Rich media available at <https://youtu.be/zvGs1aXWQnU>

Movie S2. Working process of the Double Bellows with DIDO and IEAR

Rich media available at <https://youtu.be/4ZeZQMB8YS0>

Movie S3. Experimental verification of IEAR on the Double Bellows

Here, the Double Bellows has a symmetric structure to produce bidirectional bending by alternatively inflating these two chambers (**Figure 2a** and **Figure S4**). According to Equation (1), we establish the dynamic model of the Double Bellows to obtain the theoretical pressures by analyzing its deformation geometry and the force equilibrium (**Figure 2b, c**; **Supplementary Note 2**).

The rhythmic actuation of the Double Bellows with our IEAR mechanism has different ON/OFF timings of the solenoid valves compared to the working cycle with a conventional DIDO mechanism (**Figure 2d, e**; **Figure S2d**). Following the initial actuation cycles, the Double Bellows exhibits a rapid transition and enters a steady-state pressure response (**Figure S5a, b**). Unlike DIDO, our IEAR mechanism prevents a

sharp decrease in the supplied air pressure p_{tank} during the transition. The comparative results demonstrate that our dynamic model of the Double Bellows agrees well with the experimental results under both the DIDO and IEAR mechanisms (**Figure 2f** and **Figure S6**). Such agreement suggests that our model can facilitate analysis of the actuation performance, including actuation speed and energy consumption. (see **Table 1** in Methods)

We obtain the theoretical actuation frequency and energy consumption per cycle of the Double Bellows with p_{high} ranging from 50 kPa to 100 kPa, and experimentally validate these results (**Figure 2g, h**). With the increase of p_{high} , both actuation frequencies with the DIDO and IEAR mechanisms decrease. However, the actuation frequency with our IEAR mechanism is markedly higher than that with DIDO for the full range of pressures (**Figure 2g**). At the same time, the energy consumption per cycle with IEAR is far less than that with DIDO (**Figure 2h**). For example, when $p_{high}=75$ kPa, the actuation frequency and energy consumption with DIDO are 0.49 ± 0.01 Hz and 8.08 ± 0.15 mWh \cdot cycle $^{-1}$, respectively. Our IEAR mechanism improves the actuation frequency to 0.93 ± 0.02 Hz (91.2%—) while reducing the energy consumption to 3.94 ± 0.09 mWh \cdot cycle $^{-1}$ (51.2%—). In addition, we change Δp (5, 10, 15 kPa) to investigate its influence on the actuation performance (**Figure S6**). It demonstrates that the IEAR mechanism is widely feasible in various working conditions to achieve high-speed and low-energy actuation. Also, the dynamic model of m-SPAs shows a satisfying capability of actuation performance analysis on the Double Bellows.

2.4 IEAR in m-SPAs with three chambers

To further verify the generalized feasibility of the dynamic model and our IEAR mechanism, we examine the operation in m-SPAs with three chambers—an architecture we term Triple Bellows (34.3 g, 150 mm; **Figure 3**; **Movie S4** and **5**).

Figure 3. m-SPAs with three chambers-Triple Bellows. **a** Structure of the Triple Bellows. **b** Deformation geometry of the Triple Bellows with two DOFs: bending relative to the ground and rotation above the z-axis. **c** Equivalent section force diagrams of the Triple Bellows. **d** Working flow chart of DIDO. When the conditions along the arrows are satisfied, the actuator moves to the next stage. **e** Working flow chart of IEAR. **f** Experimental pressures and theoretical pressures of DIDO and IEAR in 0-3 s. $p_{low}=10$ kPa, $\Delta p=10$ kPa. **g** Steady-state actuation frequency with p_{high} from 50 to 100 kPa. **h** Steady-state energy consumption per cycle with p_{high} from 50 to 100 kPa.

Rich media available at <https://youtu.be/cdszoIvga6s>

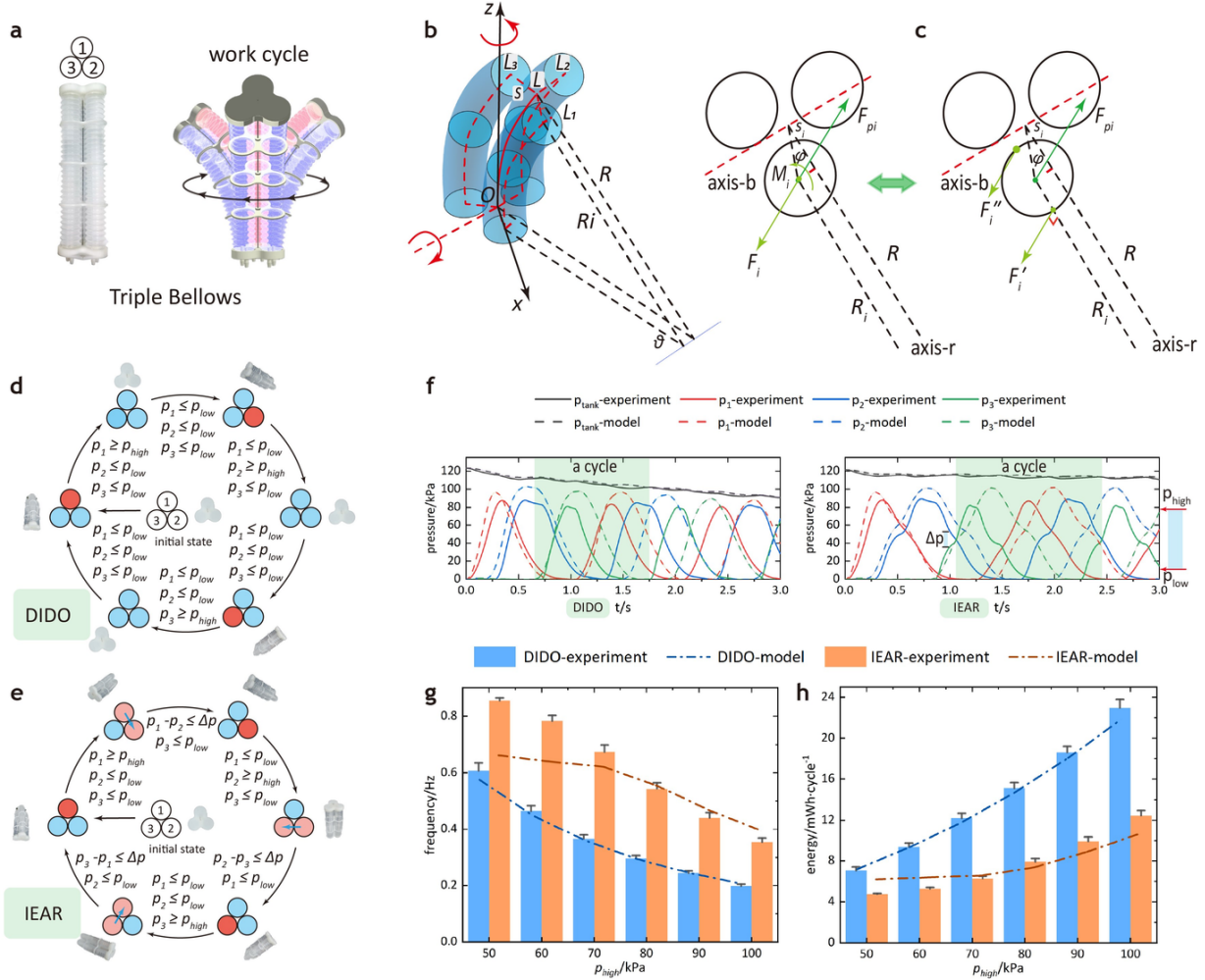
Movie S4. Working process of the Triple Bellows with DIDO and IEAR

Rich media available at https://youtu.be/S8_AzK8qmBw

Movie S5. Experimental verification of IEAR on the Triple Bellows

Compared with the Double Bellows, the Triple Bellows comprises three chambers arranged in an equilateral triangle, while other structural features remain the same (**Figure 3a** and **Figure S4**). These three chambers endow the Triple Bellows with two DOFs: bending relative to the ground and rotation above the z-axis (**Figure 3b**). According to the force equilibrium on these two DOFs, we can establish the dynamic model (**Figure 3c** and **Supplementary Note 3** and **4**). For both the DIDO and IEAR mechanisms (**Figure 3d, e**), the comparative theoretical and experimental results show good agreement with the others (**Figure 3f** and **Figure S7**).

We further characterize the actuation frequency and energy consumption per cycle of the Triple Bellows with p_{high} from 50 kPa to 100 kPa covered. According to **Figure 3g, h**, the Triple Bellows also achieve high-speed and low-energy actuation with IEAR. Taking $p_{high}=75$ kPa as an example, the actuation frequency



and energy consumption of DIDO are 0.33 ± 0.01 Hz and 13.50 ± 0.50 mWh \cdot cycle $^{-1}$, respectively. Through our IEAR mechanism, the actuation frequency is improved to 0.60 ± 0.02 Hz (82.4%—) while the energy consumption is reduced to 7.06 ± 0.27 mWh \cdot cycle $^{-1}$ (47.7%—). The results from changing Δp (5, 10, 15 kPa) again verify the dynamic model of m-SPAs and the ability of our IEAR mechanism to improve actuation speed and reduce energy consumption in various working conditions (**Figure S7**).

2.5 Applications of IEAR

2.5.1 Robotic fin

We first design a robotic fin (89.2 g) composed of two Double Bellows and a PVC sheet to verify our IEAR mechanism for applications in soft robotics (**Figure 4a-f**, **Supplementary Note 5**, and **Movie S6**). In an underwater experiment, the robotic fin swings and drags the PVC sheet to produce propulsion force, which fluctuates with different magnitudes and periods in real-time (**Figure 4c**). Experimental results show that, compared with DIDO for the full range of p_{high} , IEAR has a markedly higher swinging frequency and average propulsion force (**Figure 4d, e**), and the energy consumption with IEAR is significantly reduced (**Figure 4f**). For instance, when $p_{high} = 75$ kPa, the swinging frequency, average propulsion force and energy consumption with DIDO are 0.41 ± 0.00 Hz, 0.19 ± 0.01 N, and 9.29 ± 0.08 mWh \cdot cycle $^{-1}$, respectively. In contrast, the corresponding actuation performance with IEAR is 0.76 ± 0.01 Hz (85.4%—),

0.32 \pm 0.01 N (68.4%—), and 4.77 \pm 0.04 mWh \cdot cycle $^{-1}$ (48.7%—). These results mean the robotic fin can produce higher swimming velocity with energy-efficient IEAR when actuating underwater vehicles (Yin et al., 2016). Moreover, we observe an extra beneficial effect of IEAR that the supplied air pressure p_{tank} is improved, and the system power is reduced simultaneously, which performs conducive factors in high-speed and high-efficiency actuation (Figure S8a-c).

Figure 4. Verification on a robotic fin and a fabric-based finger. **a** The robotic fin swings in water to produce propulsion force where p_{low} = 10 kPa, Δp = 10 kPa. **b** The robotic fin comprises two Double Bellows and a PVC sheet with a thickness of 0.5 mm. **c** Propulsion force in real-time when p_{high} = 50, 75, 100 kPa, respectively. **d** Swinging frequency of the robotic fin. **e** Average propulsion force produced by the robotic fin. **f** Energy consumption per cycle of the robotic fin. **g** The fabric-based actuator is composed of a flexing chamber and an extending chamber. The actuator is worn on a silicone model hand to assist the finger. **h** Steady-state actuation frequency of the actuator. **i** Steady-state energy consumption per cycle of the actuator.

Rich media available at <https://youtu.be/BF1WUAojcvQ>

Movie S6. Application on a robotic fin

2.5.2 Fabric-based finger

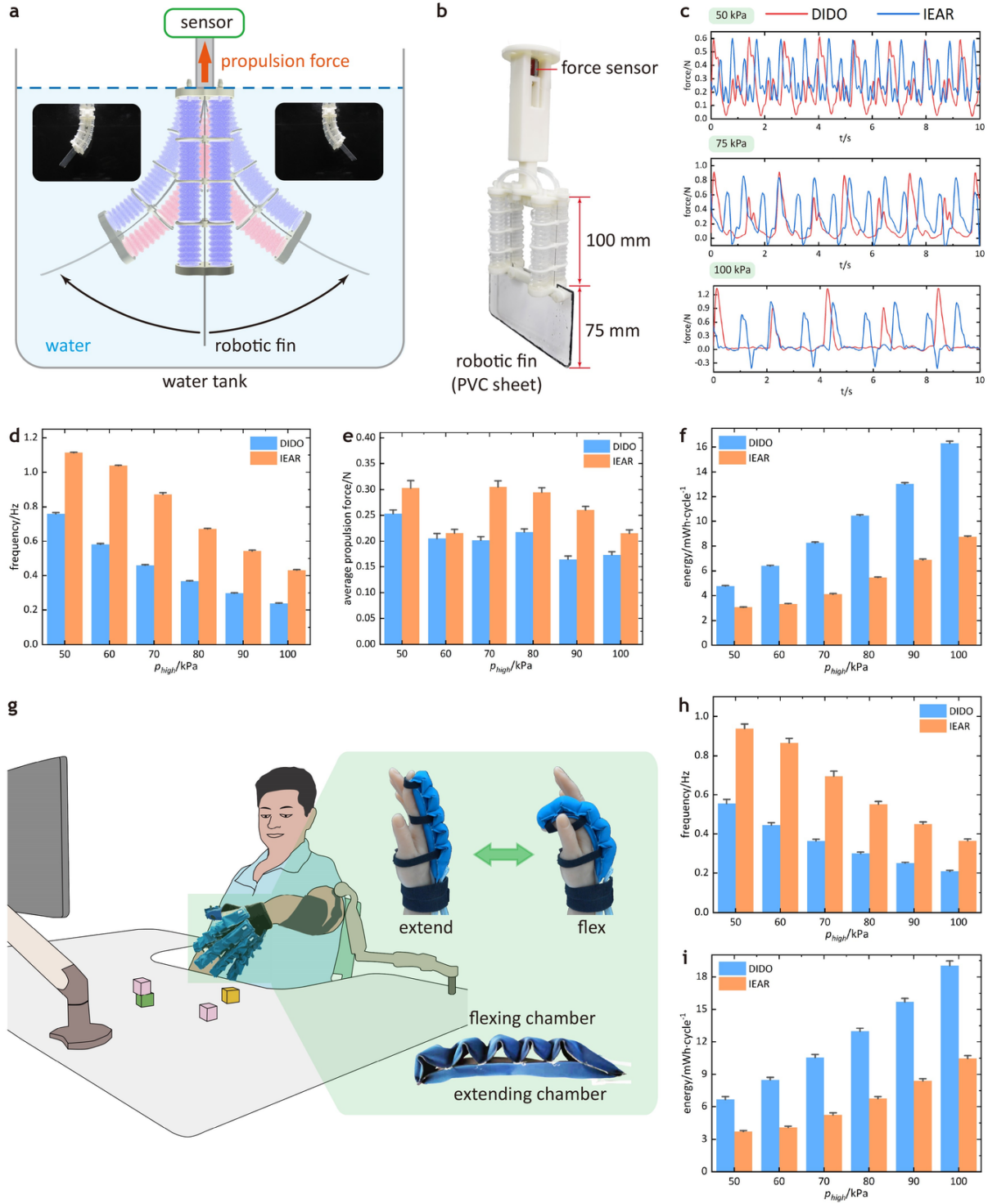
We further fabricate a soft fabric-based pneumatic actuator (Feng et al., 2021; Ge et al., 2020) for use in rehabilitation and assistive exoskeletons to examine the broad potential of IEAR for different materials and actuator types (Figure 4g-i, Supplementary Note 6, and Movie S7). This fabric-based actuator (10.2 g) comprises a flexing chamber and an extending chamber, and it is worn on a silicone hand to assist the finger motion. Experimental results show that the actuation frequency with our IEAR mechanism is nearly $2 \times$ that with DIDO for the full range of pressures, while the energy consumption per cycle only takes about half that with DIDO (Figure 4h and i). For example, when p_{high} = 75 kPa, the actuation frequency and energy consumption with DIDO are 0.33 ± 0.01 Hz and 11.70 ± 0.28 mWh \cdot cycle $^{-1}$. However, the corresponding actuation performances with IEAR are 0.62 ± 0.02 Hz (87.9%—) and 5.99 ± 0.20 mWh \cdot cycle $^{-1}$ (48.8%—). In hand rehabilitation, especially assistance, an actuation speed of faster than 0.5 Hz is important for activities of daily living (ADLs) (Polygerinos et al., 2015), such as grasping an apple, operating a ball or drinking water. Besides, the comparisons of the supplied air pressure p_{tank} and the system power also demonstrate the advantages of our IEAR over the traditional DIDO (Figure S8d-f). Except for the fabric-based finger, an extensive application on a fiber-reinforced silicone actuator also verifies the effectiveness of IEAR in improving actuation speed and energy efficiency (Figure S9a-c and Supplementary Note 7).

Rich media available at <https://youtu.be/5v7IwnAxqLY>

Movie S7. Application on a fabric-based finger

2.5.3 Quadruped robot

To verify the potential application of the Triple Bellows, we adopt an electronics-free soft-legged design (Drotman et al., 2021) and fabricate a quadruped robot (Figure 5, Supplementary Note 8, and Movie S8). The quadruped robot (244.1 g with a body length of 220 mm) constitutes four Triple Bellows, whose chambers are connected to form three groups numbered in color (Figure 5a and b). By sequentially actuating these chambers, we let the robot walk on a 900 mm floorboard and record the walking performance (Figure 5c). According to the results in Figure 5d-f, both the step frequency and walking velocity with our IEAR mechanism are markedly more than that with DIDO for the full range of pressures, while IEAR consumes much less energy per step than DIDO. Typically when p_{high} = 75 kPa, the walking time with IEAR (64.5 \pm 2.3 s) is 30.6 \pm 4.4 s shorter than that with DIDO (95.1 \pm 3.7 s), and the energy consumption per



step with IEAR ($16.53 \pm 0.82 \text{ mWh} \cdot \text{step}^{-1}$) is 39.4% less than that with DIDO ($27.27 \pm 1.42 \text{ mWh} \cdot \text{step}^{-1}$). Moreover, the steplength with DIDO is smaller than that with IEAR, which reflects the smaller air supply with the DIDO mechanism (**Figure 5f**). For the quadruped robot, the supplied air pressure p_{tank} and

system power are also slightly ameliorated (**Figure S8g-i**). Compared with the robotic fin and fabric-based glove, the large air consumption of the quadruped robot might reduce the extra improvement of p_{tank} and system power.

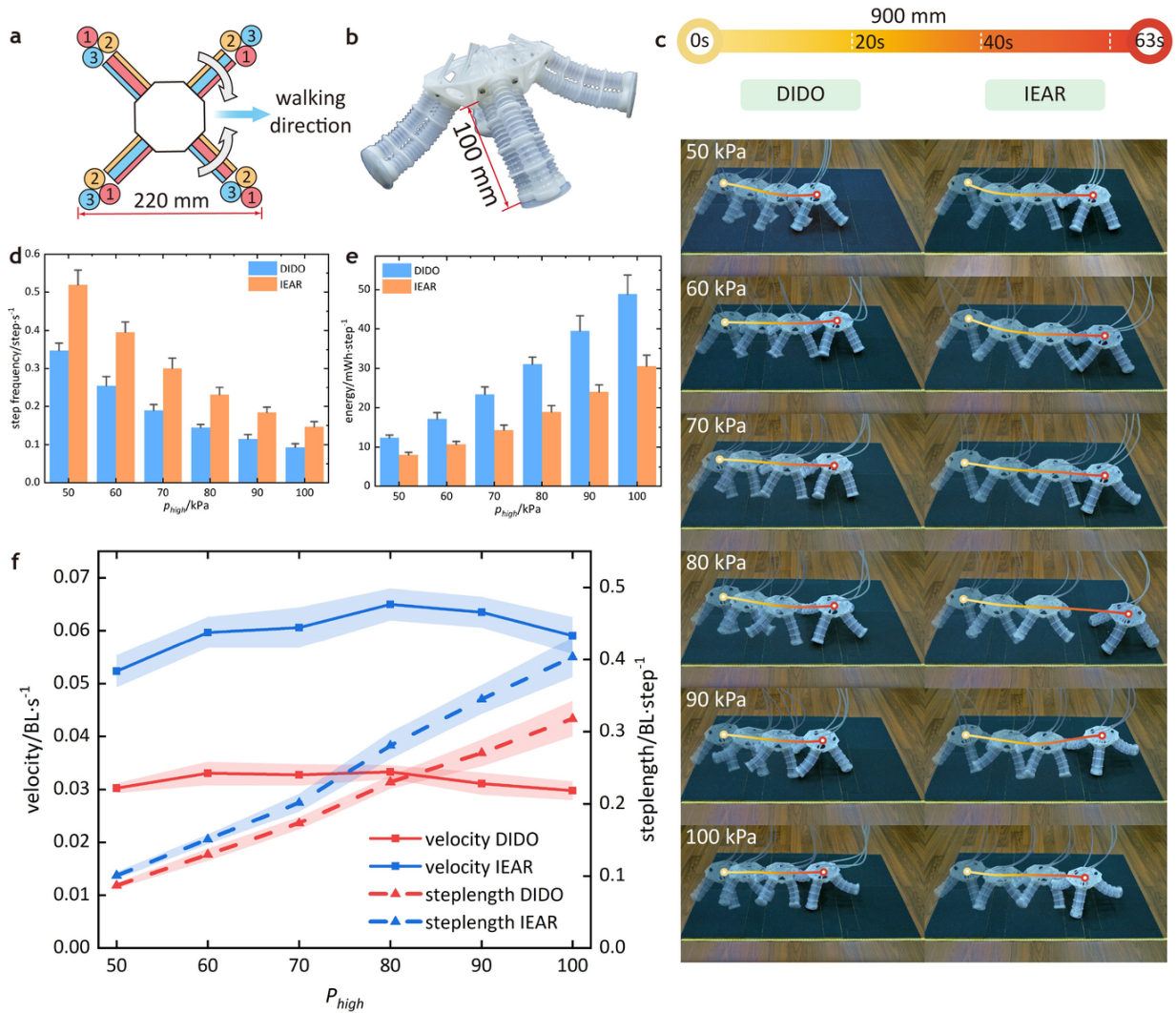


Figure 5. Verification on a quadruped robot fabricated by four Triple bellows. **a** The quadruped robot walks forward by sequentially inflating three groups of chambers. **b** Structure of the quadruped robot. **c** The quadruped robot walks on a floorboard of 900 mm in length. The graph records the crawling states at 0, 20, 40, and 63 s (the earliest time to arrive at the destination) with different p_{high} , where $p_{low} = 10$ kPa, $\Delta p = 10$ kPa. **d** Step frequency of the quadruped robot. **e** Energy consumption per step. **f** Crawling velocity and steplength.

Rich media available at <https://youtu.be/mE2qzLGEKZ0>

Movie S8. Application on a quadruped robot

3. Discussion

We present the IEAR mechanism to achieve high-speed and low-energy actuation of m-SPAs in various pneumatic soft machines and robots. A dynamic model of m-SPAs is developed to guide the analysis of the actuation mechanism, which agrees well with the experiments on the exemplary m-SPAs, the Double Bellows and the Triple Bellows. These experiments also demonstrate the ability of IEAR to improve actuation speed and reduce energy consumption. Moreover, we observe an improvement in the supplied air pressure p_{tank} and a decrease in the system power, which may result from the enhanced performance of the air supply and the reduction of required energy input to the IEAR-assisted system, respectively. Lastly, we demonstrate the practical feasibility and broad potential of IEAR with applications on a robotic fin, fabric-based finger, and quadruped robot.

As demonstrated in our experiments, the dynamic model of m-SPAs can give accurate pressure and actuation frequency. Although there are some errors, it is not easy for the dynamic pressure modeling of soft robots, especially for these m-SPAs with coupled interaction between chambers. These errors mainly come from the ignorance of actuator mass, the inaccuracy of actuator volume modeling and the inconsistency of commercial solenoid valves. Indeed, this model is generally applicable to both rigid and soft multi-chamber actuators, as long as the volume-pressure function Equation (3) can be established. Based on our dynamic model of m-SPAs and some practical models for mass flow (Joshi and Paik, 2021; Joshi et al., 2021; Cheng et al., 2018; Jungong et al., 2008; Kawashima et al., 2004; KUROSHITA, 2002; Robinson et al., 2015; Woods et al., 2014), a reverse design for air passage and actuation could be feasible and may lead to higher-performing soft machines and robots.

In this study, we present a group of comparative experiments with EEAR, where we find that IEAR performs better in improving actuation speed and energy efficiency, and the combination of IEAR and EEAR can greatly reinforce the performance of EEAR under high working pressure (**Figure S9g-k** and **Supplementary Note 9**). These experiments verify the ability of IEAR to achieve high-speed and low-energy actuation of m-SPAs. However, since the air in this study flows only between a pair of chambers at each step, further investigation is required to study simultaneous flow among a network of chambers. For a more lightweight system with IEAR, soft circuits supporting onboard control should also be investigated as a replacement for the rigid valve island by adopting soft pumps, microfluidic-activated valves, and smart fluids (McDonald and Ranzani, 2021). Thus, a wider range of soft machines and robots, including fully untethered robotic systems (Rich et al., 2018), might benefit from our IEAR mechanism.

4. Methods

4.1 Materials of the pneumatic control system

The components of the pneumatic system include a micro air pump (KZP-PE, Kamoer Fluid Tech Co., Ltd., China, **Supplementary Note 10**), a 3D-printed air tank and a valve island (DSM IMAGE8200 pro, WeNext Technology Co., Ltd., China), 12 solenoid valves (0520D, Foshan Weizi Electronic Technology Co., Ltd., China), two current sensors (Huaibei Vidias Electronic Technology Co., Ltd, China), a temperature sensor (Quanzhou Guanhangda Electronic Technology Co., Ltd, China), four pressure sensors (MPX4250DP, Freescale Semiconductor, USA), a relay (Risym, China) for the air pump, two solid-state relay panels (customized) for solenoid valves, two high-precision programmable linear power supplies (SS-L303SPV, Dong Guan Great Electronics Co., Ltd., China), and a controller (microLabBox 1202, dSPACE, Germany).

The electrical current data is used for power measurement, and the temperature sensor is inserted into the air tank to record the temperature of compressed air. In this study, the actual temperature of compressed air is generally 17-24 , and we approximate the temperature as a constant 20 for simplification, which has little influence on the results under the thermodynamic scale of temperature. For the pressure sensors, one measures p_{tank} , and the other three are assigned to p_1 , p_2 , and p_3 . All the pneumatic components and

actuators are connected by silicone tubes (Daoguan, China) with an inner diameter of 2 mm and an outer diameter of 4 mm. When the output pressure of the pump changes, the pump power varies following the experimentally obtained law (**Figure S2c**). Due to these inductive components, such as solenoid valves and pumps, the high precision programmable linear power supplies are used to avoid voltage fluctuation. In all the experiments, the sampling frequency of the system is set to 1 kHz.

4.2 Structure, materials, and fabrication of exemplary actuators

The primary materials (**Figure S4**) for fabricating the Double Bellows and the Triple Bellows are commercial PVC tubes (Yingli Plastic Co., Ltd, China), 3D-printed frames (DSM IMAGE8200 pro, WeNext Technology Co., Ltd., China), steel wires with a diameter of 0.5 mm (LXJMGSS, China), and AB epoxy resin glue (Deli Group, China). As presented in **Figure S4c**, we hypothesize that the tube is linearly elastic and experimentally obtain the stiffness using the universal testing machine (68SC-2, Instron, USA).

The Double Bellows is primarily composed of two commercial bellow-shaped PVC tubes (**Figure 2a** and **Figure S4**) capped with airtight adhesive at two ends. A pair of steel wires are introduced in the middle of the Double Bellows to keep the length of the central axis constant, which makes more length change of PVC tube convert to actuator bending. To avoid mechanical instability of the PVC tube when inflated, a group of constraint rings is inserted along the actuator body to bundle these PVC tubes and steel wires. Compared with the Double Bellows, the Triple Bellows comprises three PVC tubes arranged in an equilateral triangle (**Figure 3a** and **Figure S4**). Other structural features of the Triple Bellows keep the same as that of the Double Bellows. The tube length of both the Double Bellows and the Triple Bellows is 150 mm (To improve structure stiffness, the length in the applications is 100 mm).

The fabrication of these exemplary m-SPAs contains six steps: i) Cut PVC tubes; ii) Bundle the tube with the constraint rings; iii) Fabricate the end caps and seal the tubes with AB glue; iv) Insert and fix the steel wires; v) Waiting for the glue to cure. vi) Examine the airtightness of the actuator.

4.3 Numerical analysis of the theoretical model

The dynamic model of m-SPAs Equation (1) is a first-order matrix partial differential equation, which generally has no analytical but numerical solutions. We analyze the dynamic pressures by MATLAB and SIMULINK (The MathWorks, Inc., USA). MATLAB is used to adjust stimulation parameters and control the simulation process. SIMULINK takes charge of numerical solutions by the fixed-step solver ode14x (extrapolation) with a step size of 0.001 s. The numerical solutions include p_{tank} , p_1 , p_2 , and p_3 . The actuation frequency and pressure magnitude can be extracted from the solutions.

4.4 Calculation, characterization, and correction of mass flow

The mass flow Q_{ij} between chamber i and j depends on the pressures on both sides of the air passage and the air passage itself (**Figure S3** and **8**). Empirical formulas (Joshi and Paik, 2021; Joshi et al., 2021; Cheng et al., 2018; Jungong et al., 2008; Kawashima et al., 2004; KUROSHITA, 2002) and the lumped-parameter resistance model (Stanley et al., 2021) (mathematically similar to empirical formulas) have conveniently approximated the flow function of an air passage, which, however, work well only when the pressure on one side remains constant. In our actuator, the pressures in both chambers change rapidly. So we use a data-driven flow Q function for higher accuracy.

$$Q_{ij} = \Psi_{ij}(p_i, p_j) \quad (p_i \geq p_j) \quad (4)$$

The characterization method of flow function is presented in **Supplementary Note 11**. Since the opening and closing time of solenoid valves cannot be ignored under high-frequency actions, we refer to the work of

Xu et al. (Xu et al., 2017) and propose a time-based piecewise linear open degree function $\Gamma(t)$ to obtain the actual mass flow through correction.

$$Q = \Gamma(t) \Psi(p_{high}, p_{low}), \Gamma \propto [0, 1] \quad (5)$$

The detailed correction method is presented in **Supplementary Note 12**.

4.5 Indicators of actuation performance

The actuation performance is primarily quantified by the following four indicators: actuation frequency f , air tank pressure p_{tank} (supplied air pressure), system power P , and energy consumption per cycle e . The calculation methods are presented in **Table 1** (See **Supplementary Note 13**), where the average is obtained from a time interval after transition into steady-state actuation and N is the equivalent weighted average number of solenoid valves in use for a working cycle (**Figure S2d**). All the experimental results in this work are obtained from seven repetitive measurements.

Table 1. Calculation of the actuation performance indicators

Indicators	Theoretical	Experimental
Actuation frequency f	\bar{f}	\hat{f}
Air tank pressure p_{tank}	\bar{p}_{tank}	$\bar{\hat{p}}_{tank}$
System power P	$NP_{valve} + P_{pump}(\bar{p}_{tank})$	$\bar{\hat{P}}_{allvalve} + \bar{\hat{P}}_{pump}$
Energy consumption per cycle e	$\frac{NP_{valve} + P_{pump}(\bar{p}_{tank})}{\bar{f}}$	$\frac{\bar{\hat{P}}_{allvalve} + \bar{\hat{P}}_{pump}}{\hat{f}}$

4.6 Materials and fabrication of the robots in applications

The robotic fin (**Figure 4b**) comprises two Double Bellows and a PVC sheet (160 mm \times 75 mm \times 0.5 mm). All the frames and connectors in this application are 3D-printed (DSM IMAGE8200 pro, WeNext Technology Co., Ltd., China), including the mounting base of the force sensor (LSB201, FUTEK Advanced Sensor Technology, Inc., USA). The robotic fin, the force sensor, and the sensor mounting base are fabricated and fixed on the 6-DOFs manipulator (JAKA Zu 7, JAKA Robotics, China) to adjust and stabilize the position conveniently. Then, we immerse the robotic fin in the water tank (600 mm \times 400 mm \times 450 mm, water depth 300 mm) to investigate the actuation performance (**Figure S8a**).

The fabric-based soft finger (**Figure S8d**) is fabricated by 30D rib weft-knitted polyester fabric coated with 0.2 mm-TPU (Jiaxing Yingcheng Textile Co., Ltd, China). A laser cutter (VLS 3.50, Universal Laser Systems, USA) trims the fabric to the target CAD pattern, and then a heat-sealing machine (customized) manually seals the fabric pieces into actuators. Specific methods are referred to the work of Feng et al. (Feng et al., 2021). For the extensive application, Ecoflex 0030 (Smooth On, USA) and M 4601 (Wacker, Germany) are mixed 1:1 (mass) to cast the fiber-reinforced silicone actuator (62.1 g).

For the quadruped robot (244.1 g), a body frame connects four Triple Bellows, shown in **Figure S8g**. The body length of the quadruped robot is 220 mm, and each foot is 100 mm long (**Figure 5b**). Silicone feet (Sujie, China) are stuck on the caps of the Triple Bellows to prevent slipping.

Acknowledgements

M. Feng conceived the idea and contributed to experiments, modeling, data processing, and writing. D. Yang assisted in experiments and writing. G. Gu and C. Majidi supervised the project and contributed to the design of experiments and writing. All the authors provided feedback and agree with the final version of the manuscript.

We thank W. Wang and Y. Su for their suggestions on airflow modeling at the early stage of this work. This work was partially supported by the National Natural Science Foundation of China (Grant Nos. 52025057 and 91948302) and the Science and Technology Commission of Shanghai Municipality (Grant No. 20550712100).

Conflict of interest

The authors declare no conflict of interest.

Supporting Information

Please refer to <https://doi.org/10.22541/au.166426480.06273183/v1> for the Supporting Information.

References

- Alar Ainla, Mohit S. Verma, Dian Yang, and George M. Whitesides. Soft, rotating pneumatic actuator. *Soft Robot*, 4(3):297–304, 2017. doi: 10.1089/soro.2017.0017.
- Cameron A. Aubin, Benjamin Gorissen, Edoardo Milana, Philip R. Buskohl, Nathan Lazarus, Geoffrey A. Slipper, Christoph Keplinger, Josh Bongard, Fumiya Iida, Jennifer A. Lewis, and Robert F. Shepherd. Towards enduring autonomous robots via embodied energy. *Nature*, 602(7897):393–402, 2022. doi: 10.1038/s41586-021-04138-2.
- Vito Cacucciolo, Jun Shintake, Yu Kuwajima, Shingo Maeda, Dario Floreano, and Herbert Shea. Stretchable pumps for soft machines. *Nature*, 572(7770):516–519, 2019. doi: 10.1038/s41586-019-1479-6.
- Shitong Chen, Feifei Chen, Zizheng Cao, Yusheng Wang, Yungeng Miao, Guoying Gu, and Xiangyang Zhu. Topology optimization of skeleton-reinforced soft pneumatic actuators for desired motions. *IEEE-ASME Trans. Mechatron.*, 26(4):1745–1753, 2021. doi: 10.1109/TMECH.2021.3071394.
- Xiaoxia Cheng, Linglong Du, Gang Yang, and Baoren Li. Adaptive robust control of dynamic gas pressure in a vacuum servo system. *Vacuum*, 148:184–194, 2018. ISSN 0042207X. doi: 10.1016/j.vacuum.2017.11.012.
- Ching-Ping Chou and B. Hannaford. Measurement and modeling of McKibben pneumatic artificial muscles. *IEEE Trans. Robot. Autom.*, 12(1):90–102, 1996. doi: 10.1109/70.481753.
- Fionnuala Connolly, Diana A. Wagner, Conor J. Walsh, and Katia Bertoldi. Sew-free anisotropic textile composites for rapid design and manufacturing of soft wearable robots. *EXTREME MECH. LETT.*, 27: 52–58, 2019. doi: 10.1016/j.eml.2019.01.007.

- Corrado de Pascali, Giovanna Adele Naselli, Stefano Palagi, Rob B. N. Scharff, and Barbara Mazzolai. 3D-printed biomimetic artificial muscles using soft actuators that contract and elongate. *Sci. Robot.*, 7(68): eabn4155, 2022. doi: 10.1126/scirobotics.abn4155.
- Raphael Deimel and Oliver Brock. A novel type of compliant and underactuated robotic hand for dexterous grasping. *Int. J. Robot. Res.*, 35(1-3):161–185, 2016. doi: 10.1177/0278364915592961.
- R. S. Diteesawat, T. Helps, M. Taghavi, and J. Rossiter. Electro-pneumatic pumps for soft robotics. *Sci. Robot.*, 6(51):eabc3721, 2021. doi: 10.1126/scirobotics.abc3721.
- Dylan Drotman, Saurabh Jadhav, Mahmood Karimi, Philip Zonia, and Michael T. Tolley. 3d printed soft actuators for a legged robot capable of navigating unstructured terrain. In *2017 IEEE International Conference on Robotics and Automation (ICRA)*, pages 5532–5538. IEEE, 2017. doi: 10.1109/ICRA.2017.7989652. URL <http://ieeexplore.ieee.org/servlet/opac?punumber=7960754>.
- Dylan Drotman, Saurabh Jadhav, David Sharp, Christian Chan, and Michael T. Tolley. Electronics-free pneumatic circuits for controlling soft-legged robots. *Sci. Robot.*, 6(51):eaay2627, 2021. doi: 10.1126/scirobotics.aay2627.
- Miao Feng, Dezhi Yang, and Guoying Gu. High-force fabric-based pneumatic actuators with asymmetric chambers and interference-reinforced structure for soft wearable assistive gloves. *IEEE Robot. Autom. Lett.*, 6(2):3105–3111, 2021. doi: 10.1109/LRA.2021.3062588.
- Lisen Ge, Feifei Chen, Dong Wang, Yifan Zhang, Dong Han, Tao Wang, and Guoying Gu. Design, modeling, and evaluation of fabric-based pneumatic actuators for soft wearable assistive gloves. *Soft Robot*, 7(5): 583–596, 2020. doi: 10.1089/soro.2019.0105.
- Tim Giffney, Mengying Xie, Aaron Yong, Andrew Wong, Philippe Mousset, Andrew McDaid, and Kean Aw. Soft pneumatic bending actuator with integrated carbon nanotube displacement sensor. *Robotics*, 5(1):7, 2016. doi: 10.3390/robotics5010007.
- Xiangyu Gong, Ke Yang, Jingjin Xie, Yanjun Wang, Parth Kulkarni, Alexander S. Hobbs, and Aaron D. Mazzeo. Rotary Actuators Based on Pneumatically Driven Elastomeric Structures. *Adv. Mater.*, 28(34): 7533–7538, 2016. doi: 10.1002/adma.201600660.
- Zheyuan Gong, Xi Fang, Xingyu Chen, Jiahui Cheng, Zhixin Xie, Jiaqi Liu, Bohan Chen, Hui Yang, Shihan Kong, Yufei Hao, Tianmiao Wang, Junzhi Yu, and Li Wen. A soft manipulator for efficient delicate grasping in shallow water: Modeling, control, and real-world experiments. *Int. J. Robot. Res.*, 40(1): 449–469, 2021. doi: 10.1177/0278364920917203.
- Benjamin Gorissen, Dominiek Reynaerts, Satoshi Konishi, Kazuhiro Yoshida, Joon-Wan Kim, and Michael de Volder. Elastic Inflatable Actuators for Soft Robotic Applications. *Adv. Mater.*, 29(43), 2017. doi: 10.1002/adma.201604977.
- Guoying Gu, Ningbin Zhang, Haipeng Xu, Shaoting Lin, Yang Yu, Guohong Chai, Lisen Ge, Houle Yang, Qiwen Shao, Xinjun Sheng, Xiangyang Zhu, and Xuanhe Zhao. A soft neuroprosthetic hand providing simultaneous myoelectric control and tactile feedback. *Nat. Biomed. Eng.*, 2021. doi: 10.1038/s41551-021-00767-0.
- Ryman Hashem, Shahab Kazemi, Martin Stommel, Leo K. Cheng, and Weiliang Xu. A biologically inspired ring-shaped soft pneumatic actuator for large deformations. *Soft Robot*, 2021a. doi: 10.1089/soro.2021.0013.
- Ryman Hashem, Martin Stommel, Leo K. Cheng, and Weiliang Xu. Design and characterization of a bellows-driven soft pneumatic actuator. *IEEE-ASME Trans. Mechatron.*, 26(5):2327–2338, 2021b. doi: 10.1109/TMECH.2020.3037643.

- Sagar Joshi and Jamie Paik. Pneumatic supply system parameter optimization for soft actuators. *Soft Robot*, 8(2):152–163, 2021. doi: 10.1089/soro.2019.0134.
- Sagar Joshi, Harshal Sonar, and Jamie Paik. Flow path optimization for soft pneumatic actuators: towards optimal performance and portability. *IEEE Robot. Autom. Lett.*, 6(4):7949–7956, 2021. doi: 10.1109/LRA.2021.3100626.
- Ma Jungong, Chen Juan, Zhao Ke, and Mitsuru Senoo. Flow-rate characteristics parameters of pneumatic component. In *Proc. of the IEEE Int. on Automation and Logistics*, pages 2946–2949. IEEE, 2008. doi: 10.1109/ICAL.2008.4636681.
- Kenji Kawashima, Yukio Ishii, Tatsuya Funaki, and Toshiharu Kagawa. Determination of flow rate characteristics of pneumatic solenoid valves using an isothermal chamber. *J. Fluids Eng.-Trans. ASME*, 126(2):273–279, 2004. doi: 10.1115/1.1667888.
- Xingxing Ke, Jiajun Jang, Zhiping Chai, Haochen Yong, Jiaqi Zhu, Han Chen, Chuan Fei Guo, Han Ding, and Zhigang Wu. Stiffness preprogrammable soft bending pneumatic actuators for high-efficient, conformal operation. *Soft Robot*, 2021. doi: 10.1089/soro.2020.0207.
- Sangjoon J. Kim, Handdeut Chang, Junghoon Park, and Jung Kim. Design of a portable pneumatic power source with high output pressure for wearable robotic applications. *IEEE Robot. Autom. Lett.*, 3(4):4351–4358, 2018. doi: 10.1109/LRA.2018.2864823.
- Kiyoshi KUROSHITA. STUDY ON MEASUREMENT METHOD OF FLOW-RATE CHARACTERISTICS OF PNEUMATIC SOLENOID VALVE. *Proceedings of the JFPS International Symposium on Fluid Power*, 2002(5-1):73–78, 2002. doi: 10.5739/isfp.2002.73. URL <https://doi.org/10.5739%2Fisfp.2002.73>.
- Sinyoung Lee, Dongun Lee, and Dongjun Shin. An air recirculation system based on bioinspired soft Re-Air valve for highly efficient pneumatic actuation. *Soft Robot*, 8(5):564–576, 2021. doi: 10.1089/soro.2020.0007.
- Haili Li, Jiantao Yao, Pan Zhou, Xinbo Chen, Yundou Xu, and Yongsheng Zhao. High-force soft pneumatic actuators based on novel casting method for robotic applications. *Sens. Actuator A-Phys.*, 306:111957, 2020. doi: 10.1016/j.sna.2020.111957.
- J. H. Low, J. Y. Goh, N. Cheng, P. M. Khin, Q. Q. Han, and C. H. Yeow. A bidirectional 3d-printed soft pneumatic actuator and graphite-based flex sensor for versatile grasping*. In *2020 IEEE International Conference on Robotics and Automation (ICRA)*, pages 7979–7985. IEEE, 2020. doi: 10.1109/ICRA40945.2020.9196837.
- Ming Luo, Mahdi Agheli, and Cagdas D. Onal. Theoretical modeling and experimental analysis of a pressure-operated soft robotic snake. *Soft Robot*, 1(2):136–146, 2014. doi: 10.1089/soro.2013.0011.
- Andrew D. Marchese, Cagdas D. Onal, and Daniela Rus. Autonomous soft robotic fish capable of escape maneuvers using fluidic elastomer actuators. *Soft Robot*, 1(1):75–87, 2014. doi: 10.1089/soro.2013.0009.
- Kevin McDonald and Tommaso Ranzani. Hardware Methods for Onboard Control of Fluidically Actuated Soft Robots. *Front. Robot. AI*, 8:720702, 2021. doi: 10.3389/frobt.2021.720702.
- Bobak Mosadegh, Panagiotis Polygerinos, Christoph Keplinger, Sophia Wennstedt, Robert F. Shepherd, Unmukt Gupta, Jongmin Shim, Katia Bertoldi, Conor J. Walsh, and George M. Whitesides. Pneumatic Networks for Soft Robotics that Actuate Rapidly. *Adv. Funct. Mater.*, 24(15):2163–2170, 2014. doi: 10.1002/adfm.201303288.
- Manabu Okui, Yuki Nagura, Yasuyuki Yamada, and Taro Nakamura. Hybrid pneumatic source based on evaluation of air compression methods for portability. *IEEE Robot. Autom. Lett.*, 3(2):819–826, 2018. doi: 10.1109/LRA.2018.2792145.

- Panagiotis Polygerinos, Zheng Wang, Kevin C. Galloway, Robert J. Wood, and Conor J. Walsh. Soft robotic glove for combined assistance and at-home rehabilitation. *Robot. Auton. Syst.*, 73:135–143, 2015. doi: 10.1016/j.robot.2014.08.014.
- Panagiotis Polygerinos, Nikolaus Correll, Stephen A. Morin, Bobak Mosadegh, Cagdas D. Onal, Kirstin Petersen, Matteo Cianchetti, Michael T. Tolley, and Robert F. Shepherd. Soft Robotics: Review of Fluid-Driven Intrinsically Soft Devices; Manufacturing, Sensing, Control, and Applications in Human-Robot Interaction. *Adv. Eng. Mater.*, 19(12):1700016, 2017. doi: 10.1002/adem.201700016.
- Daniel J. Preston, Haihui Joy Jiang, Vanessa Sanchez, Philipp Rothemund, Jeff Rawson, Markus P. Nemitz, Won-Kyu Lee, Zhigang Suo, Conor J. Walsh, and George M. Whitesides. A soft ring oscillator. *Sci. Robot.*, 4(31):eaaw5496, 2019. doi: 10.1126/scirobotics.aaw5496.
- Xinda Qi, Hongyang Shi, Thassyo Pinto, and Xiaobo Tan. A novel pneumatic soft snake robot using traveling-wave locomotion in constrained environments. *IEEE Robot. Autom. Lett.*, 5(2):1610–1617, 2020. doi: 10.1109/LRA.2020.2969923.
- Steven I. Rich, Robert J. Wood, and Carmel Majidi. Untethered soft robotics. *Nat. Electron.*, 1(2):102–112, 2018. doi: 10.1038/s41928-018-0024-1.
- Matthew A. Robertson, Hamed Sadeghi, Juan Manuel Florez, and Jamie Paik. Soft pneumatic actuator fascicles for high force and reliability. *Soft Robot*, 4(1):23–32, 2017. doi: 10.1089/soro.2016.0029.
- Ryan M. Robinson, Curt S. Kothera, and Norman M. Wereley. Variable recruitment testing of pneumatic artificial muscles for robotic manipulators. *IEEE-ASME Trans. Mechatron.*, 20(4):1642–1652, 2015. doi: 10.1109/TMECH.2014.2341660.
- Robert F. Shepherd, Filip Ilievski, Wonjae Choi, Stephen A. Morin, Adam A. Stokes, Aaron D. Mazzeo, Xin Chen, Michael Wang, and George M. Whitesides. Multigait soft robot. *Proc. Natl. Acad. Sci. U. S. A.*, 108(51):20400–20403, 2011. doi: 10.1073/pnas.1116564108.
- Jun Shintake, Vito Cacucciolo, Dario Floreano, and Herbert Shea. Soft robotic grippers. *Adv. Mater.*, page e1707035, 2018. doi: 10.1002/adma.201707035.
- Saivimal Sridar, Souvik Poddar, Yida Tong, Panagiotis Polygerinos, and Wenlong Zhang. Towards untethered soft pneumatic exosuits using low-volume inflatable actuator composites and a portable pneumatic source. *IEEE Robot. Autom. Lett.*, 5(3):4062–4069, 2020. doi: 10.1109/LRA.2020.2986744.
- Andrew A. Stanley, Amirhossein Amini, Casey Glick, Nathan Usevitch, Yiğit Mengüç, and Sean J. Keller. Lumped-Parameter Response Time Models for Pneumatic Circuit Dynamics. *J. Dyn. Syst. Meas. Control-Trans. ASME*, 143(5), 2021. doi: 10.1115/1.4049009.
- Constantinos Stergiopoulos, Daniel Vogt, Michael T. Tolley, Michael Wehner, Jabulani Barber, George M. Whitesides, and Wood, Robert J., A Soft Combustion-Driven Pump for Soft Robots. A Soft Combustion-Driven Pump for Soft Robots. In *Proceedings of the ASME 2014 Conference on Smart Materials, Adaptive Structures and Intelligent Systems*. ASME, 2014. doi: 10.1115/SMASIS2014-7536.
- Ken Takaki, Yoshitaka Taguchi, Satoshi Nishikawa, Ryuma Niiyama, and Yoshihiro Kawahara. Acoustic length sensor for soft extensible pneumatic actuators with a frequency characteristics model. *IEEE Robot. Autom. Lett.*, 4(4):4292–4297, 2019. doi: 10.1109/LRA.2019.2931273.
- Michael T. Tolley, Robert F. Shepherd, Bobak Mosadegh, Kevin C. Galloway, Michael Wehner, Michael Karpelson, Robert J. Wood, and George M. Whitesides. A resilient, untethered soft robot. *Soft Robot*, 1(3):213–223, 2014. doi: 10.1089/soro.2014.0008.
- Yuanyuan Wang, Shota Kokubu, Zhongchao Zhou, Xinyao Guo, Ya-Hsin Hsueh, and Wenwei Yu. Designing soft pneumatic actuators for thumb movements. *IEEE Robot. Autom. Lett.*, 6(4):8450–8457, 2021. doi: 10.1109/LRA.2021.3105799.

- Michael Wehner, Michael T. Tolley, Yiğit Mengüç, Yong-Lae Park, Annan Mozeika, Ye Ding, Cagdas Onal, Robert F. Shepherd, George M. Whitesides, and Robert J. Wood. Pneumatic energy sources for autonomous and wearable soft robotics. *Soft Robot*, 1(4):263–274, 2014. doi: 10.1089/soro.2014.0018.
- Michael Wehner, Ryan L. Truby, Daniel J. Fitzgerald, Bobak Mosadegh, George M. Whitesides, Jennifer A. Lewis, and Robert J. Wood. An integrated design and fabrication strategy for entirely soft, autonomous robots. *Nature*, 536(7617):451–455, 2016. doi: 10.1038/nature19100.
- Benjamin K. S. Woods, Curt S. Kothera, Gang Wang, and Norman M. Wereley. Dynamics of a pneumatic artificial muscle actuation system driving a trailing edge flap. *Smart Mater. Struct.*, 23(9):095014, 2014. doi: 10.1088/0964-1726/23/9/095014.
- Haifan Wu, Ato Kitagawa, Hideyuki Tsukagoshi, and Canghai Liu. Development of a Novel Pneumatic Power Assisted Lower Limb for Outdoor Walking by the Use of a Portable Pneumatic Power Source: Singapore, 1 - 3 October 2007 ; [part of IEEE Multi-Conference on Systems and Control, MSC. In *16th IEEE Int. Conf. on Control Applications*, pages 1291–1296. IEEE Service Center, 2007. doi: 10.1109/CCA.2007.4389413.
- Matheus S. Xavier, Andrew J. Fleming, and Yong, Yuen K., Modelling and Simulation of Pneumatic Sources for Soft Robotic Applications. Modelling and Simulation of Pneumatic Sources for Soft Robotic Applications. In *2020 IEEE/ASME International Conference on Advanced Intelligent Mechatronics (AIM)*, pages 916–921. ASME, 2020. doi: 10.1109/AIM43001.2020.9158802.
- Matheus S. Xavier, Andrew J. Fleming, and Yuen Kuan Yong. Design and Control of Pneumatic Systems for Soft Robotics: A Simulation Approach. *IEEE Robot. Autom. Lett.*, 6(3):5800–5807, 2021. doi: 10.1109/LRA.2021.3086425.
- Matheus S. Xavier, Charbel D. Tawk, Ali Zolfagharian, Joshua Pinski, David Howard, Taylor Young, Jiewen Lai, Simon M. Harrison, Yuen K. Yong, Mahdi Bodaghi, and Andrew J. Fleming. Soft Pneumatic Actuators: A Review of Design, Fabrication, Modeling, Sensing, Control and Applications. *IEEE Access*, 10:59442–59485, 2022. doi: 10.1109/ACCESS.2022.3179589.
- Xiangyang Xu, Xiao Han, Yanfang Liu, Yanjing Liu, and Yang Liu. Modeling and dynamic analysis on the direct operating solenoid valve for improving the performance of the shifting control system. *Appl. Sci.*, 7(12):1266, 2017. doi: 10.3390/app7121266.
- Hee Doo Yang, Brandyn T. Greczek, and Alan T. Asbeck. Modeling and Analysis of a High-Displacement Pneumatic Artificial Muscle With Integrated Sensing. *Front. Robot. AI*, 5:136, 2018. doi: 10.3389/frobt.2018.00136.
- Hong Kai Yap, Hui Yong Ng, and Chen-Hua Yeow. High-force soft printable pneumatics for soft robotic applications. *Soft Robot*, 3(3):144–158, 2016. doi: 10.1089/soro.2016.0030.
- Xinyan Yin, Lichao Jia, Chen Wang, and Guangming Xie. Modelling of thrust generated by oscillation caudal fin of underwater bionic robot. *Appl. Math. Mech.*, 37(5):601–610, 2016. doi: 10.1007/s10483-016-2074-8.
- Sung-Sik Yun, Brian Byunghyun Kang, and Kyu-Jin Cho. Exo-Glove PM: an easily customizable modularized pneumatic assistive glove. *IEEE Robot. Autom. Lett.*, 2(3):1725–1732, 2017. doi: 10.1109/LRA.2017.2678545.
- Boyu Zhang, Jiaqi Chen, Xin Ma, Yi Wu, Xinran Zhang, and Hongen Liao. Pneumatic System Capable of Supplying Programmable Pressure States for Soft Robots. *Soft robotics*, 2021. doi: 10.1089/soro.2021.0016.
- Gabriel Zoller, Vincent Wall, and Oliver Brock. Acoustic sensing for soft pneumatic actuators: 2018 IEEE/RSJ International Conference on Intelligent Robots and Systems : October, 1-5, 2018, Madrid, Spain, Madrid Municipal Conference Centre. In *2018 IEEE/RSJ International Conference on Intelligent Robots and Systems (IROS)*, pages 6986–6991. IEEE, 2018. doi: 10.1109/IROS.2018.8594396. URL <http://ieeexplore.ieee.org/servlet/opac?punumber=8574473>.